Mon. Not. R. Astron. Soc. **000**, 000–000 (0000) Printed 2 February 2008 (MN LaTeX style file v2.2)

arXiv:astro-ph/0407359v1 16 Jul 2004

Host Galaxies of Gamma-Ray Bursts and their Cosmological Evolution

Stéphanie Courty, Gunnlaugur Björnsson, Einar H. Gudmundsson
Science Institute, University of Iceland, Dunhaga 3, IS–107 Reykjavik, Iceland
`e-mail: courty, gulli, einar@raunvis.hi.is`

2 February 2008

ABSTRACT

We use numerical simulations of large scale structure formation to explore the cosmological properties of Gamma-Ray Burst (GRB) host galaxies. Among the different sub-populations found in the simulations, we identify the host galaxies as the most efficient star-forming objects, i.e. galaxies with high specific star formation rates. We find that the host candidates are low-mass, young galaxies with low to moderate star formation rate. These properties are consistent with those observed in GRB hosts, most of which are sub-luminous, blue galaxies. Assuming that host candidates are galaxies with high star formation rates would have given conclusions inconsistent with the observations. The specific star formation rate, given a galaxy mass, is shown to increase as the redshift increases. The low mass of the putative hosts makes them difficult to detect with present day telescopes and the probability density function of the specific star formation rate is predicted to change depending on whether or not these galaxies are observed.

Key words: cosmology: large-scale structure of the Universe – galaxies: formation – galaxies: evolution – gamma rays: bursts

1 INTRODUCTION

For three decades Gamma-Ray Bursts (GRBs) remained an enigma. The detection of optical afterglows associated with a GRB (see van Paradijs et al. 2000, for a review), revolutionized our understanding of the phenomena. A GRB is now thought to occur when the core of a massive star collapses to form a black hole (Woosley 1993; Paczyński 1998; MacFadyen & Woosley 1999) (see also Mészáros 2002, for a review). In most cases when an optical afterglow from a GRB has been detected, they have been shown to occur in galaxies at intermediate or high redshifts. To date, the redshift of over 40 GRB afterglows and their host galaxies have been measured. Because of the short lifetime of a massive star, a GRB is generated essentially instantaneously after the star's formation, as compared to the evolutionary timescale of a typical galaxy or the cosmological timescale. The bursts are therefore generally considered to be good tracers of the history of massive star formation (e.g. Blain & Natarajan 2000).

It was early realized that because of their extreme brightness, GRBs and their afterglows might be detectable to very high redshifts and therefore might be useful as cosmological probes, in particular if the bursts possessed a 'standard candle' like property (e.g. Lamb & Reichart 2000). The main interest in the cosmological application of GRBs has resulted from the increased understanding of the relation between GRBs and powerful supernovae (e.g. Hjorth et al. 2003; Stanek et al. 2003) and from there the mapping of the cosmic star formation history (e.g. Ramirez-Ruiz et al. 2002, and references therein). Other possible applications have also been considered, such as the use of bursts as probes of the interstellar medium in evolving galaxies and as probes of primordial star formation and reionization, although these are observationally very challenging at present (e.g. Djorgovski et al. 2003). Constructing a reliable Hubble diagram with GRB afterglows, however, is likely to remain a very difficult subject (Bloom et al. 2003).

In this paper, we take a different approach altogether. Instead of focusing on the diverse properties of the bursts themselves we use the fact that in almost all cases where sufficiently deep observations have been carried out, a host galaxy has been discovered. Many of the host galaxies are very faint, with R band magnitudes down to about 30 (Jaunsen et al. 2003), and might have gone undetected had not a GRB occurred in them. We will occasionally refer to the hosts as *GRB selected* galaxies. Unfortunately, the number of hosts is still too limited for statistical studies, but this is likely to change after *Swift* is launched in 2004. A number of first results on the hosts does exist however, and a picture of their properties is beginning to emerge. The host morphology shows most of them to be dwarf galaxies, either compact, irregular or interacting, possibly merging, and they also tend to be blue in color (e.g. Bloom et al. 1998; Le Floc'h et al. 2003; Berger et al. 2003). Many hosts are sub-luminous, with $L/L_* < 1$, (e.g. Le Floc'h et al. 2003), with GRB 990705 a notable exception (Le Floc'h et al. 2002). The star formation rate (SFR) in most hosts as inferred from optical observations show low to intermediate activity, with $SFR = 1 - 50 M_\odot/\mathrm{yr}$ (e.g. Bloom et al. , 1999; Castro-Tirado et al. 2001; Fynbo et al. 2001; Chary et al. 2002; Price et al. 2002). In a number of cases the sub-mm and radio observations indicate a SFR that is up to a factor of 10 higher than the optically inferred rates (Berger et al. 2003). Finally, Sokolov et al. (2001) and Chary et al. (2002) infer a host galaxy mass, M, typically in the range $2 \cdot 10^8 - 4 \cdot 10^{10} M_\odot$. In addition, the variation in the specific star formation rate, SFR/M, from host to host is modest, normally within a factor of a few (Chary et al. 2002; Christensen et al. 2004). In fact, Christensen et al. (2004) has shown that all the hosts in their sample have spectral energy distributions similar to young starburst galaxies with small to moderate extinction. Comparing their sample with the Hubble Deep Field, they find the hosts to be similar to the bluest of the field galaxies which have the highest specific SFR.

As the bursts occur in galaxies, they can be viewed not only as tracers of massive star formation, but also as tracers of galaxy formation and evolution. The study of GRBs and their host galaxies is therefore intimately linked to the study of galaxy evolution in general. Although the presently known host sample indicates that bursts can occur in any type of galaxy, the majority of them are faint and show a dwarf-like morphology. They may therefore belong to the faint end of the galaxy luminosity function. GRB selected galaxies may prove to be an important sub-population of the galaxy population and their study may thus provide information about the galaxy luminosity function not easily accessible otherwise.

The aim of this paper is to investigate theoretically the properties of the host galaxies of GRBs as well as their cosmological evolution rather than to focus on the GRB progenitor and its properties. To this end, we use numerical simulations of large scale structure formation with the aim of identifying objects in the simulations with properties corresponding to those observed in the hosts. The simulations we use, were previously considered by Alimi & Courty (2004) to explore a number of galaxy properties such as the cosmic star formation rate density and the galaxy mass function. The simulations reveal a significant population of low-mass galaxies whose existence raises a number of questions on galaxy evolution. In this paper we concentrate on the instantaneous and the specific star formation rates of the simulated galaxies. We identify a sub-population of the galaxies with high specific star formation rate as the likely candidates for GRB hosts. We find that the majority of this putative host population has low-mass and low to modest SFR, although a number of high-mass objects also have similar specific rates. We then explore the properties and cosmic evolution of the simulated host population and compare to the galaxy population as a whole.

In section 2, we describe the details of the numerical simulations relevant for this study. In section 3 we introduce the instantaneous star formation rate and in particular the specific star formation rate as a measure of the efficiency of star formation. We also discuss the properties of the general galaxy population at low redshift. In section 4 a similar discussion is presented for high redshift and the cosmological evolution of the galaxy properties is explored. In section 5 we propose interpretations of the observations and we argue that GRB host galaxies may be a powerful tracer of the faint galaxy population. Section 6 concludes the paper.

2 NUMERICAL SIMULATIONS

The simulations were performed with a 3D N-body/hydrodynamical code, coupling a PM scheme for computing gravitational forces with an Eulerian approach for solving the hydrodynamical equations. Shock heating is treated with the artificial viscosity method (Von Neumann & Richtmyer 1950). The radiative cooling processes included are: collisional excitation, collisional ionization, recombination, bremsstrahlung and Compton scattering. Collisional ionization equilibrium is not assumed and the cooling rates are computed from the evolution of a primordial composition hydrogen-helium plasma. The simulations also include a model for galaxy formation, summarized below. The numerical procedures are described in more detail in Courty & Alimi (2004) and Alimi & Courty (2004). The galaxy properties discussed in the latter paper were found to be consistent with observational data. This suggests that the galaxy formation model used here to investigate the nature of host galaxies of GRBs, captures the essence of the galaxy formation process.

Numerical simulations of large scale structure formation do not currently allow following the formation of objects of mass lower than the scale of a grid cell, a few times $10^6\ M_\odot$. But computing the thermodynamic properties of the gas and its cosmological evolution allow us to consider the physical conditions needed to form a galaxy. The most important condition is that the gas cloud is collapsing, in the sense that the cooling time is less than the dynamical time or the free fall time (Rees & Ostriker 1977). We then identify, at each time step, gas regions satisfying this condition. A fraction of the gas mass is turned into an object, labeled a "stellar particle", with a rate:

$$\frac{\mathrm{d}m_B}{\mathrm{d}t} = -\frac{m_B}{t_*}, \tag{1}$$

with $m_B(t)$ the available baryonic mass enclosed within the gas region at cosmic time t, and t_* a characteristic timescale. The cosmological evolution of these particles is followed in a non-collisional way. To express the condition $t_{\rm cool} < t_{\rm ff}$, we define the cooling timescale $t_{\rm cool}$, computed from the internal energy variation of the gas, and the dynamical time or free fall time, $t_{\rm ff} = \sqrt{3\pi/32G\rho}$. To make sure that gas regions giving birth to galaxies are correctly identified we use additional criteria: the size of the gas cloud must be less than the Jean's length given by $\lambda_J = c_s(\pi/G\rho)^{1/2}$; the gas must be in a converging flow: $\nabla \cdot \vec{v} < 0$; the baryonic density contrast, $\delta_B \equiv (\delta\rho/\bar{\rho})_B$, must be higher than a threshold $(1+\delta_B)_s$, here taken to be the value of the baryonic density contrast at the turnaround, i.e. 5.5 as computed in the top-hat collapse spherical model (Padmanabhan 1993). The total matter density, including dark matter, baryonic matter and stellar particles, is used in the expressions for the dynamical time and the Jean's length. In each cell, checking that the four criteria described above are satisfied, a fraction $\Delta t/t_*$ of the gas is turned into a stellar particle, with Δt the timestep of the simulation. If a stellar particle starts forming at cosmic time t_0 when the baryonic mass enclosed within the grid cell is $m_B(t_0)$, we assume that the particle is fully formed at time $t_i = t_0 + \Delta t$. Using eq. (1), we find that the final mass of the particle is given by

$$m_i = m_B(t_0) - m_B(t_i) \simeq m_B(t_0)\frac{\Delta t}{t_*}. \qquad (2)$$

The characteristic time is taken to be $t_* = \max(t_{\rm ff}, 10^8 \text{ yr})$. The stellar particles are involved in the computation of the gravitational potential and their evolution is treated in the same way as the collisionless dark matter.

Galaxy-like objects are then defined, at any redshift, by grouping the stellar particles with a friend-of-friend algorithm. This algorithm joins together all particles closer than a distance proportional to a link parameter η, usually taken to be 0.2 (equivalent to selecting an overdensity of 187 in the spherical collapse model). The mass range of the stellar particles spans from 10^6 to 10^8 $M_\odot$, but in what follows we only consider, at any redshift, galaxies with a total mass higher than $5 \cdot 10^8 M_\odot$, although a number of lower mass galaxies also form in the simulations. At $z = 0$, this lower galaxy mass limit corresponds to a minimum of 11 stellar particles per galaxy and at $z = 3$ it corresponds to a minimum of 27 particles. The total number of galaxy objects in the catalogs at $z = 0$, 1 and 3 are 1650, 2164 and 1602, respectively.

Through the formation of the stellar particles and their groupings we therefore have access to the formation history of each galaxy at any redshift. The mass of the galaxy at any time is the sum of the mass of its individual stellar particles at that time. This mass is likely to be an estimate of all the stellar populations formed over the lifetime of the galaxy, as the dark matter component is not included in the galaxy mass. We estimate the epoch of formation for a given galaxy as the mean epoch of formation of all stellar particles the galaxy is composed of, weighted by the mass of each particle, i.e. $t_{\rm m1} = \sum(m_i t_i)/\sum m_i$, where t_i is the cosmic time corresponding to the epoch of formation of stellar particle i. An alternative method would be to define the formation epoch as the epoch, $t_{\rm m2}$, at which the galaxy has acquired half of its final mass. Both methods give similar epoch estimates as shown in Figure 1. As the former method is based on the formation history of the stellar populations that make up the galaxy, it resembles the way galaxy ages are estimated observationally, namely from the age of the stellar populations in the galaxy. In this work, all formation epochs are therefore estimated with the first method.

The results of this paper are given for a $\Lambda-$cold dark matter model. The parameters of the simulations are: $H_0 = 70$ km s^{-1} Mpc^{-1}, $\Omega_K = 0$, $\Omega_m = 0.3$, $\Omega_\Lambda = 0.7$, $\Omega_b = 0.02h^{-2}$ with $h = H_0/100$. The initial density fluctuation spectrum uses the transfer functions taken from Bardeen et al. (1986) with a shape parameter given by Sugiyama (1995). The fluctuation spectrum is normalized on COBE data (Bunn & White 1997) leading to a filtered dispersion at $R = 8$ h^{-1} Mpc of $\sigma_8 = 0.91$. The resolution of the simulations is as follows: the number of dark matter particles is $N_p = 256^3$ and the number of grid cells is $N_g = 256^3$; the comoving size of the computational volume is $L_{box} = 32$ $h^{-1} Mpc$, giving a dark matter particle mass of 2.01×10^8 $M_\odot$, and a gas mass initially enclosed in each grid cell of 3.09×10^7 $M_\odot$.

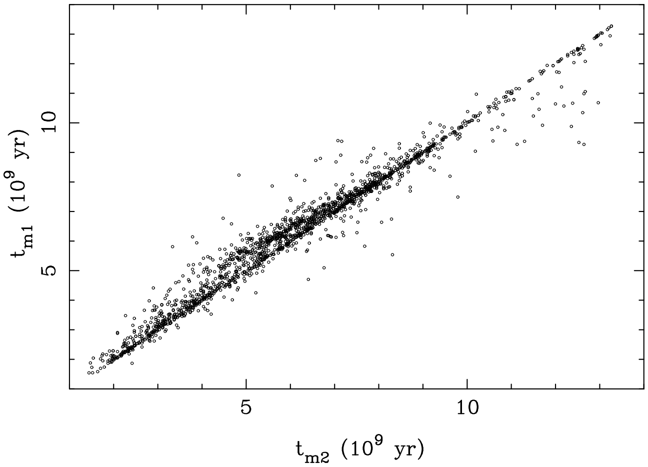

Figure 1. Comparing the two different ways of estimating the epoch of formation of galaxies, $t_{\rm m1}$ and $t_{\rm m2}$, computed from the galaxy catalog at $z = 0$. See text for definitions.

3 INSTANTANEOUS STAR FORMATION RATE AND EFFICIENCY OF STAR FORMATION

For each object at any given redshift z, corresponding to cosmic time t_z, we compute the instantaneous star formation rate SFR^*, where $*$ indicates a value obtained from the simulations. The instantaneous rate is computed from the mass in stellar populations in the galaxy that have age less than τ at time t_z, $SFR^* = \Delta M/\tau$. This is equivalent to the baryonic mass ΔM, having been converted to stars during time τ prior to the epoch under consideration. Note that the SFR^* depends both on τ and the cosmic time, $SFR^*(\tau, t_z)$. It depends also on the amount of gas in the galaxy that is available for star formation at t_z since the star formation rate in the model is proportional to the baryonic density. We use $\tau = 0.1$ Gyrs as representative value at $z = 0$, time dilated at higher redshifts. Figure 2 shows a comparison between SFR^* computed with $\tau = 0.05$ and $\tau = 0.1$ Gyrs for galaxies in the catalog at $z = 3$. Also indicated in the figure are the masses of the objects as explained in the caption. We note that the star formation rates appear to be rather insensitive to the adopted value of τ, indicating that for most of the simulated galaxies, the SFR^* is rather constant over a timescale of 0.1 Gyrs at high redshift (see also Weinberg et al. (2002) for similar comparisons). There is some dispersion in the two estimates, mainly due to irregularities in the star formation events in a given galaxy. In addition, some galaxies that have a non-zero SFR^* as computed with $\tau = 0.1$ Gyrs, show no star formation on shorter timescales. These galaxies are also shown in fig. 2, but assigned an arbitrary value of $SFR^*(\tau = 0.05) = 0.03$ $M_\odot$/yr. For the low-mass objects with the lowest SFR^*, there is an

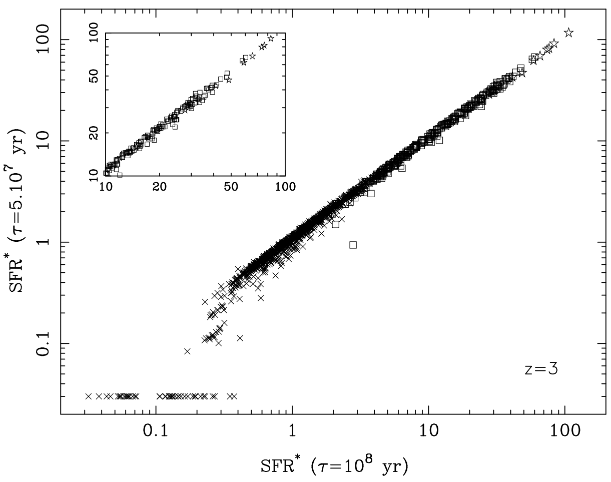

Figure 2. Comparison between the instantaneous star formation rates, in units of $M_\odot$/yr, computed for time dilated values of $\tau = 0.1$ Gyrs and $\tau = 0.05$ Gyrs for the catalog at $z = 3$. Galaxies with $SFR^* = 0.0$ at $\tau = 0.05$ Gyrs are plotted at $SFR^* = 0.03$. Symbols denote the mass range of each galaxy: $5 \cdot 10^8 - 5 \cdot 10^9 M_\odot$ (crosses), $5 \cdot 10^9 - 10^{11} M_\odot$ (squares), $M > 10^{11} M_\odot$ (stars). The inset shows a blow-up of the highest SFR^*-range.

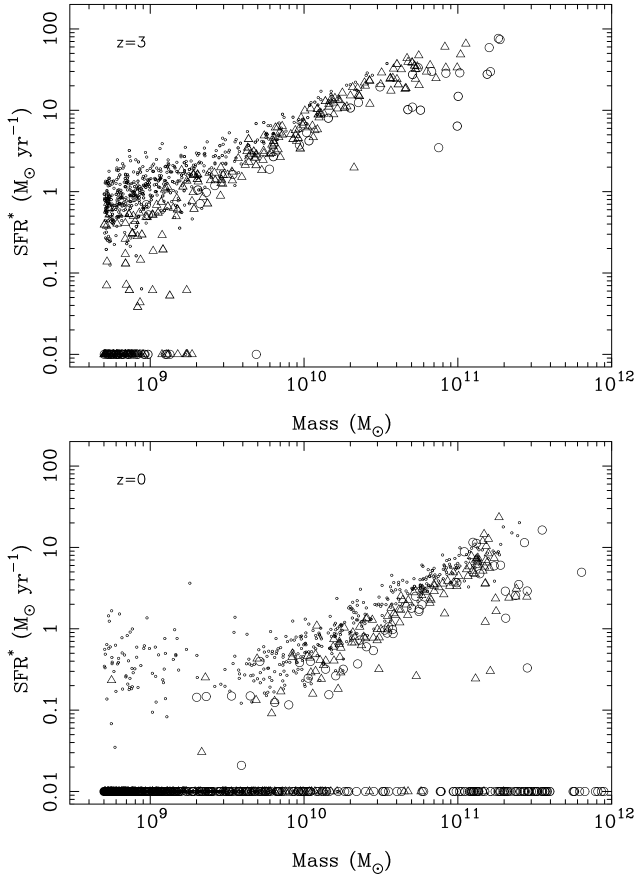

Figure 3. Instantaneous star formation rate as a function of galaxy mass, computed with $\tau = 0.1$ Gyrs, for the catalogs at $z = 3$ (upper panel) and $z = 0$ (lower panel). For clarity, only 1000 objects with non-zero SFR^* are plotted from the catalog at $z = 3$. The symbols indicate the epoch of formation of each galaxy. In the upper panel they denote: epoch of formation less than $z = 3.9$ (dots), epochs in the range $z = 3.9 - 4.3$ (triangles) and epochs greater than 4.3 (open circles). In the lower panel we have: less than $z = 0.9$ (dots), in the range $z = 0.9 - 1.1$ (triangles) and greater than $z = 1.1$ (open circles). In both panels galaxies with $SFR^* = 0.0$ are plotted at $SFR^* = 0.01$ $M_\odot$/yr.

apparent trend for the lower value of τ to yield a lower value of SFR^*, up to a a factor of a few. The larger value of τ samples a longer period of star formation in the galaxy prior to the epoch under consideration and may therefore include periods of stronger star formation activity, resulting in a higher SFR^*.

Figure 3 shows the SFR^* as a function of the mass of the objects for the catalogs at $z = 0$ and $z = 3$. Galaxies with non-zero SFR^* are plotted arbitrarily at $SFR^* = 0.01$ $M_\odot$/yr. In the former catalog, 572 objects have non-zero SFR^* for $\tau = 0.1$ Gyrs, while in the latter these objects are 1470, but for clarity only 1000 randomly selected objects with non-zero SFR^* are plotted. Also indicated in fig. 3 are three ranges of the epoch of formation of the galaxies. For the catalog at $z = 0$, the dividing epochs are $z = 0.9$, and $z = 1.1$, roughly corresponding to half and the third of the age of the Universe. For the catalog at $z = 3$, we use $z = 3.9$ and $z = 4.3$ as the dividing epochs. For both redshifts, the instantaneous star formation rate increases linearly with mass although there is considerable dispersion especially at the lower redshift. For $z = 0$, this linearity holds only in the approximate mass range $10^{10} - 10^{11} M_\odot$, for lower masses there is a large scatter in the SFR^*. For the higher redshift the linearity extends over two decades in mass. It is clear at both redshifts that the older objects tend to have lower SFR^* than the younger objects and a slightly steeper mass dependence than linear, though the difference decreases with increasing redshift.

Note also, that galaxies of a given mass tend to have up to 10 times higher SFR^* at $z = 3$ than at $z = 0$ and that the maximum SFR^* in the catalogs decreases with redshift from about 100 $M_\odot$/yr at $z = 3$ to about 10-20 $M_\odot$/yr at $z = 0$. It is interesting to note that these high SFR^* values at high redshift are consistent with the observationally inferred SFR of Lyman-break galaxies at $z = 3$ (Giavalisco 2002). The evolution of SFR^* with redshift is very weak for the low-mass objects in fig. 3, as their SFR^* tends to stay constant in time. The most dramatic difference in the cosmological evolution of the SFR^* is seen in high-mass, old galaxies. The oldest (open circles) and most massive objects have a SFR^* up to two orders of magnitudes lower than their younger counterparts (dots). In fact, the star formation rate of massive, early-formed galaxies at $z = 0$ is similar to that of the population of low-mass objects (few times $10^9 M_\odot$ or less), almost all of which are late-formed galaxies.

Note that the plots in fig. 3 show a number of galaxies which are not forming stars at the time of observation, t_z. In these objects star formation has already ceased or may be temporally stopped. These objects, although inactive, are quite numerous with most of them being of low-mass at both redshifts but being of higher mass as the redshift decreases. At low redshift, most of the massive galaxies show no activity at all. These high-mass, inactive galaxies reside in the center of the most massive dark matter halos (Alimi & Courty 2004) and, as the evolution progresses, the

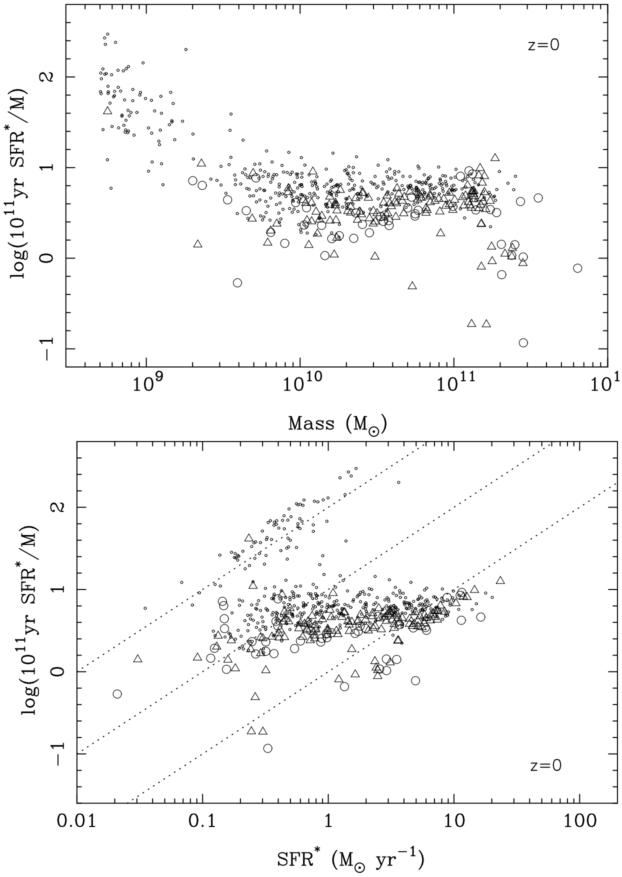

Figure 4. Upper panel: Efficiency parameter ϵ, as a function of galaxy mass for the catalog at $z = 0$. Compare also with fig. 3, where the different symbols are explained. Lower panel: ϵ as a function of SFR^* for galaxies in the catalog at $z = 0$. The dotted lines indicate a constant mass of $10^9, 10^{10}$ and $10^{11} M_\odot$ (from left to right).

depth of the potential wells prevents more and more gas from cooling. This hierarchical character of the galaxy formation process results in a strongly reduced star formation activity at low redshift, and resembles that observed in elliptical galaxies in the center of galaxy clusters. Adopting a higher value of τ would indeed cause some of these massive, early-formed galaxies to have a non-zero SFR^* (recall fig. 2) as it would take into account the latest formed stellar populations, in the case where there is still some cold gas available. This inactive population is important for our understanding of galaxy evolution and will be discussed further in Section 5.

The amount of gas turned into stars at any given epoch, t_z, depends on the amount of cold gas available in a gas region, hence the scaling of the SFR^* with the mass of a galaxy. However, a low-mass galaxy can be more efficient in turning gas into stars than a high-mass galaxy. A measure of this efficiency is given by the specific star formation rate, the ratio of the SFR^* to the mass of the galaxy. The specific star formation rate is usually normalized to a given mass, and we define a star formation efficiency parameter ϵ by,

$$\epsilon \equiv \log\left(\frac{SFR^*}{M_\odot \mathrm{yr}^{-1}}\right)\left(\frac{M}{10^{11} M_\odot}\right)^{-1}$$

$$= \log(10^{11}\mathrm{yr}\, SFR^*/M). \qquad (3)$$

Although ϵ is a dimensionless parameter we will use it and the specific star formation rate, interchangeably and with the same meaning. In fig. 4, we plot ϵ as a function of mass in the upper panel and as a function of SFR^* in the lower panel, for galaxies in our catalog at $z = 0$. In the lower panel, galaxies of a given mass are located along diagonal lines, three of which are shown. It is apparent that the low mass galaxies have a much higher specific star formation rate than intermediate or high-mass galaxies and are therefore much more efficient in turning baryonic mass into stellar mass. In fact, the old and very high-mass objects, $M > 10^{11}\ M_\odot$, and some of the older intermediate mass objects, have specific rates that are up to two orders of magnitudes lower than the low-mass objects ($M < 10^{10}\ M_\odot$). The results presented in the upper panel show a similar trend as seen in observational studies on blue compact galaxies (Guzman et al. 1997) and star-forming galaxies (Pérez-González et al. 2003), where the specific star formation rate is seen to increase with decreasing galaxy mass for low-mass galaxies, $M < 10^{10}\ M_\odot$. Despite approximations and a number of uncertainties inherent in numerical simulations, we find that our specific rates agree quite well with the observationally inferred values. The low-mass objects are observed to have ϵ in the range $1.25 - 3$ (Guzman et al. 1997), where we find the range to be about $1 - 2.5$ in the simulations.

The lower panel of fig. 4 reveals several interesting properties of the galaxy population. It is apparent that the galaxies tend to cluster in different regions in this figure. Most of the objects in the intermediate mass range, have an efficiency in the range $\epsilon = 0 - 1$, although there is a clear difference between the young and the old objects, the younger ones in general being more efficient. The star formation activity of these intermediate mass objects, as defined by their star formation rate, spans the range $SFR^* = 0.1 - 20\ M_\odot/\mathrm{yr}$. Another interesting feature seen in fig. 4 are the two distinct groups of objects, one of high-mass with low efficiency ($\epsilon \lesssim 0$), and the other of low-mass but with high efficiency ($\epsilon > 1$). The low-mass objects, that cluster around the diagonal line representing a galaxy mass of $10^9 M_\odot$, have the highest specific star formation rate, but only an SFR^* in the approximate range $0.1 - 1\ M_\odot/\mathrm{yr}$. The most massive objects, although again spanning almost two orders of magnitude in their SFR^*, distinguish themselves by having by far the lowest specific star formation rate. In general terms, we thus see that the low-mass objects are the most efficient in their star formation, by a factor of 10 over the intermediate class. The most massive ones are again a factor of at least $5 - 10$ less efficient than the intermediate ones.

We present in figure 5 a statistical quantification of the star formation efficiency of the galaxy population at $z = 0$, where we have computed the number of objects in a bin of ϵ. The dotted histogram in both panels represents all galaxies in the catalog. This distribution peaks around $\epsilon \approx 0.7$, with considerable tails extending both above and below the peak. In the upper panel, the solid histogram shows the corresponding distribution for all objects more massive than $5 \cdot 10^{10}\ M_\odot$. The distribution is now cut off above $\epsilon \approx 1.0$, clearly demonstrating that it is the lower mass range of objects that have the highest star formation efficiency at

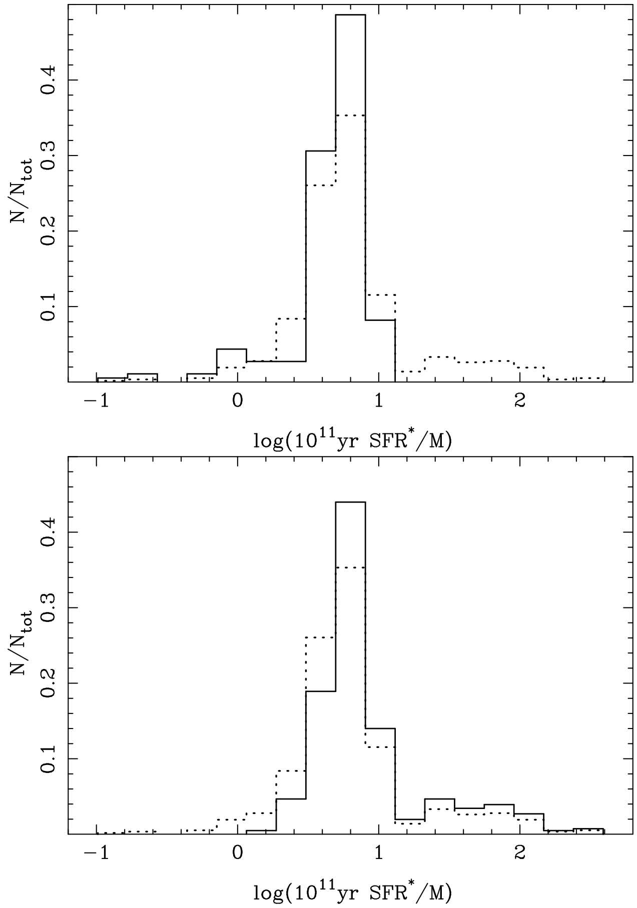

Figure 5. Distribution of galaxies per bin of ϵ for galaxies in the catalog at $z = 0$. The dotted histograms, representing all galaxies in the catalog, are identical in both panels. The solid histogram in the upper panel is for galaxies more massive than $5 \cdot 10^{10}\ M_\odot$, while the solid histogram in the lower panel is for objects with epoch of formation less than $z = 0.9$. All histograms are normalized to the number of objects in each distribution.

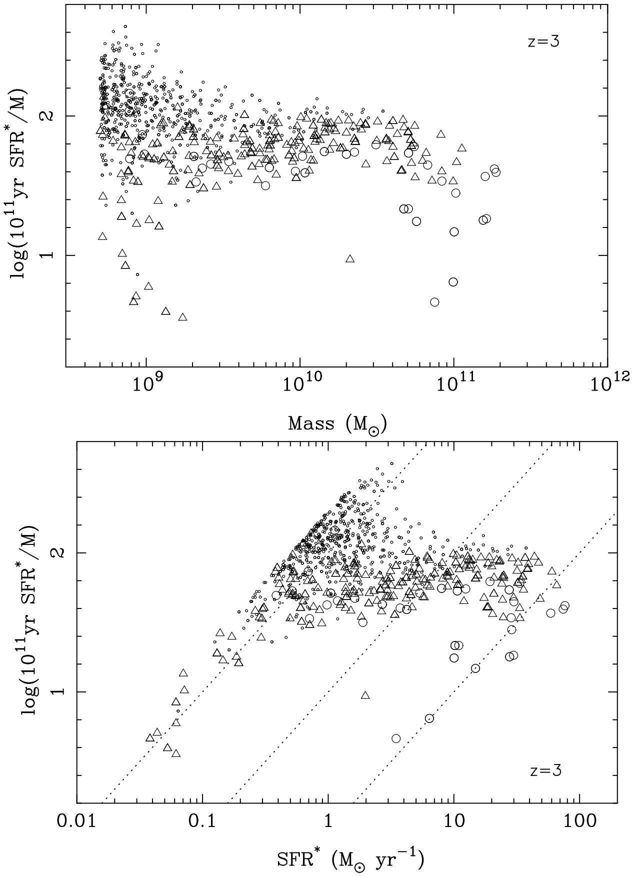

Figure 6. Efficiency parameter, ϵ, of galaxies in the catalog at $z = 3$ as a function of mass (upper panel), and as a function of SFR^* (lower panel). For clarity, only 1000 objects are plotted in each panel. As in fig. 3, the dots denote formation epochs lower than $z = 3.9$, triangles denote epochs in the range $z = 3.9 - 4.3$, and circles denote formation epochs higher than 4.3. The dotted lines in the lower panel indicate a constant mass of $10^9, 10^{10}$ and $10^{11} M_\odot$ (from left to right).

present. The solid histogram in the lower panel of fig. 5 displays the corresponding distribution if only recently formed galaxies are included (epoch of formation less than $z = 0.9$). The main difference between the young population and the total is that the objects with low star formation efficiency have disappeared. Comparing the two panels, it is apparent that the low mass objects have the highest star formation efficiency (upper panel) and the lowest efficiency is generally found in the oldest objects (lower panel). In the following discussion we will denote the peak value of a given catalog by $\bar{\epsilon}$, and refer to objects with $\epsilon > \bar{\epsilon}$, as efficiently star-forming galaxies. Similarly, galaxies with $\epsilon < \bar{\epsilon}$ will be termed inefficient.

4 COSMOLOGICAL EVOLUTION

The star formation activity of the galaxy population evolves strongly with redshift as seen in fig. 3. This evolution is also manifest in the cosmic evolution of the star formation rate density (see Hopkins et al. (2001) for a compilation of observational data). Observations show a strongly decreasing star formation activity towards lower redshifts for $z \lessapprox 2$, while its evolution towards high redshift is much less certain. The actual star formation rate in a given galaxy not only depends on the history of the galaxy, but also on merger events, environment, etc. In this section we explore the evolution with redshift of the star formation properties discussed in the previous section. As the cosmic star formation activity decreases for redshifts below $z = 2$, we consider mainly the catalogs of objects at $z = 0$ and $z = 3$ for this exploration.

In fig. 6, we show ϵ as a function of mass and star formation rate for the galaxies in the catalog at $z = 3$. This should be compared to fig. 4, but note the different vertical scale. The efficiency is essentially constant over most of the mass range and the greatest dispersion is for objects with mass less than a few times $10^9 M_\odot$. The distribution of ϵ is much narrower than at $z = 0$, and the mean value is also considerably higher, $\epsilon \approx 1.8$, an indication of the strong cosmological evolution of the efficiency of star formation. This trend has also been seen in observational data (Guzman et al. 1997; Brinchmann & Ellis 2000). In the lower panel in fig. 6, we see that the clear separation of the galaxies into distinct groups or regions observed at $z = 0$, is nearly absent at $z = 3$.

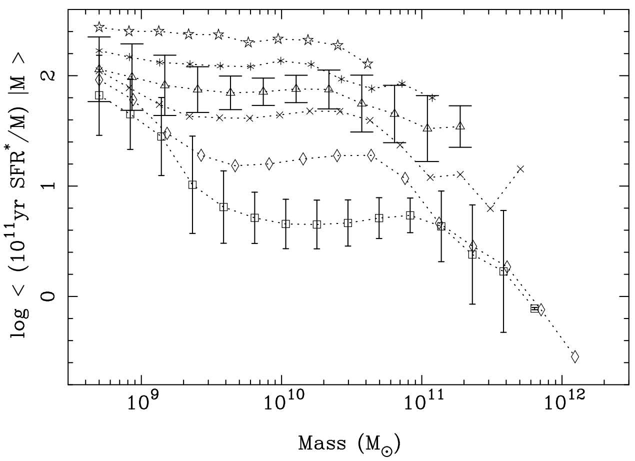

Figure 7. Conditional mean of having a specific star formation rate at a given mass, $\langle SFR/M|M\rangle$, as a function of mass at different redshifts: $z = 0$ (squares), $z = 1$ (diamonds), $z = 2$ (crosses), $z = 3$ (triangles), $z = 4$ (stars), $z = 5$ (open stars); for clarity, error bars representing dispersion around the mean are only plotted at $z = 0$ and $z = 3$.

The diagram does show the presence of a sub-population of low-mass objects with high efficiency but a moderate SFR^*. This population is not clearly separated from the intermediate mass objects at this redshift, but it continues to be present at $z = 0$ with only slightly lower efficiency and activity. Comparing with fig. 4, we note another interesting result, the appearance at low redshift of the high-mass objects with low efficiency and low SFR^*. Note also that at both redshifts, the highest mass objects always have the highest SFR^*.

In fig. 7 we show the conditional mean of having a specific star formation rate at a given mass as a function of mass and its evolution with redshift. So as not to clutter the diagram too much we only show the dispersion around the mean for the catalogs at $z = 0$ and $z = 3$. In general the dispersion is less at higher redshifts except for the low-mass objects as already noted in fig. 6. The largest difference in ϵ between low and high-mass galaxies is seen at low redshift, where only the low-mass and some of the intermediate mass objects have high specific star formation rate. At high redshift the entire galaxy population has a high specific rate. It is apparent from the figure that the specific star formation rate of the lowest mass objects decreases only slightly from $z = 5$ to $z = 0$, whereas for the intermediate to high-mass objects it decreases by two orders of magnitudes or more. It is clear that the low-mass objects are not only the most efficient ones at $z = 0$ as already noted, they are efficient at all redshifts. At higher redshifts the difference between the efficiency of the different mass ranges diminishes, but the star formation efficiency of the low-mass objects is consistent with being constant out to a redshift of 5.

5 DISCUSSION

Numerical simulations provide us with catalogs of galaxy-like objects characterized by different properties such as mass, epoch of formation and star formation rate. Galaxy sub-populations in the catalogs are clearly distinct especially at low redshift, e.g. the high-mass population with low star formation rate contrasting with the efficient low-mass population. The former population shows a decreasing star formation activity with lower redshifts. As mentioned in section 3, a number of objects at low redshift have a zero value of SFR^* when measured over a time τ. To make the picture of our simulated galaxy population complete, we show in the upper panel of fig. 8, the entire population at $z = 1$ as a function of mass and epoch of formation. In this section we focus on the redshift $z = 1$, as it is close to the peak of the current GRB redshift distribution and most of the observed host galaxies have redshifts around unity. The catalog at $z = 0$ shows the same trends as is easily verified by comparing the lower panels in figs. 8 and 4. In figure 8, stars refer to the inactive galaxy population that has no measurable SFR^* at this redshift. Most of this population is either low-mass galaxies or high-mass galaxies. We note also that these objects are quite old. Among the active galaxy population (square symbols), galaxies with a non-

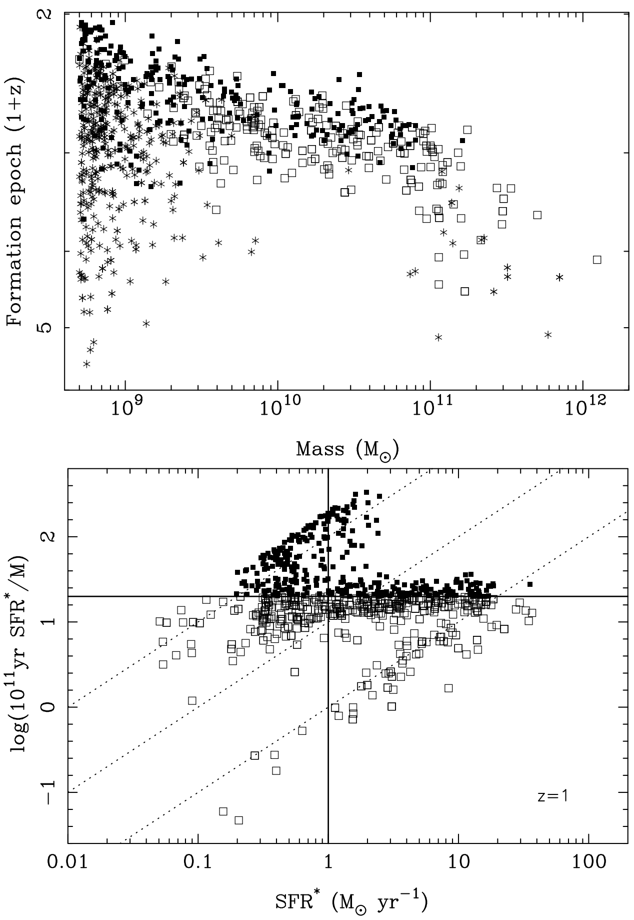

Figure 8. Upper panel: Galaxy sub-populations at $z = 1$ as a function of mass and epoch of formation. Stars denote inactive galaxies ($SFR^* = 0$), and squares active galaxies ($SFR^* > 0$), with empty symbols for inefficient and filled ones for efficient galaxies (at this redshift the dividing efficiency is $\bar{\epsilon} = 1.3$). Lower panel: Star formation efficiency, ϵ, of the active population in the catalog at $z = 1$ as a function of SFR^*. For clarity only 1000 randomly selected objects are plotted in both panels. As in previous figures, the dotted lines indicate constant masses of $10^9, 10^{10}$ and $10^{11} M_\odot$ (from left to right).

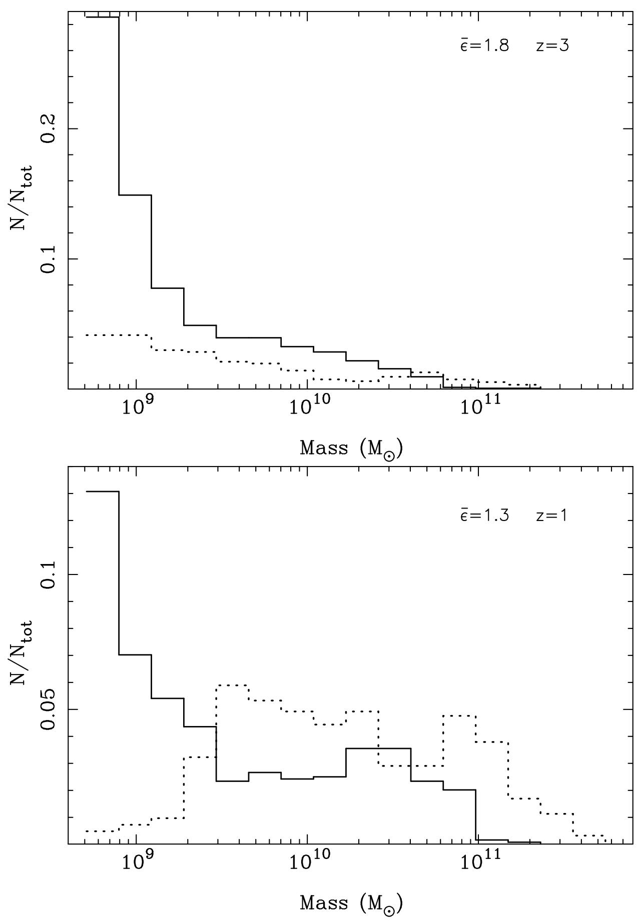

Figure 9. Number of galaxies per bin of mass at redshift of $z = 3$ (upper panel) and $z = 1$ (lower panel). In each panel the solid histogram shows the distribution of the efficient population (with $\epsilon > \bar{\epsilon} = 1.8$ at $z = 3$ and $\epsilon > \bar{\epsilon} = 1.3$ at $z = 1$) and the dotted histogram shows the non-efficient population (with $\epsilon < 1.8$ at $z = 3$ and $\epsilon < 1.3$ at $z = 1$). Both histograms are normalized on the whole population.

zero SFR^* (1239 objects) are separated in the upper panel of fig. 8 into an efficient population, including all galaxies with $\epsilon > \bar{\epsilon} = 1.3$ (filled squares), and an inefficient population with $\epsilon < \bar{\epsilon} = 1.3$ (open squares). The most efficient galaxies are low-mass and late-formed galaxies as already pointed out in the previous sections. The lower panel of fig. 8 focuses on the active population in a ϵ vs. SFR^* diagram. This plot (as the one at $z = 0$ in fig. 4) reveals again that high star formation rate galaxies are not necessarily galaxies with the highest specific SFR^*. This kind of representation emphasizes the distinction between the star formation activity (SFR^*, along the horizontal axis) and the star formation efficiency (ϵ, along the vertical axis), as two different measures of the process of converting baryons into stars.

The efficient and inefficient populations are statistically characterized at high and low redshifts in fig. 9 where we show their distribution per bin of mass. Note that both distributions at each redshift are normalized on the whole population, so adopting lower or higher values of $\bar{\epsilon}$ would alter the shape of both the efficient and inefficient populations. At $z = 3$, most of the objects with star formation efficiency above $\bar{\epsilon} = 1.8$ (solid histogram) are low-mass objects ($M <$ a few times $10^9\, M_\odot$). High-mass objects are not very numerous at this redshift (cf. fig. 6), and most of them are inefficient. At $z = 1$ most of the efficient objects are again predominantly of low-mass, although a considerable fraction of intermediate mass objects (approximately $10^{10} - 10^{11} M_\odot$) also have high efficiency. The non-efficient objects at $z = 1$, are dominated by the mass range of few times $10^9\, M_\odot$ to almost $10^{12}\, M_\odot$. At the lower redshift, essentially all of the low-mass objects are efficient in their star formation. The same can be said about the corresponding distribution at $z = 0$, almost all low-mass objects are efficient. To summarize, we note that efficient galaxies exist over almost the entire mass range at high redshift (see also fig. 7). At low redshift the efficiency becomes strongly mass dependent, as is also clear from the lower panel in fig. 4. Most importantly, the efficient population is dominated by a large number of low-mass objects, independent of the redshift. Considering the lower panels of figs. 6 and 8, we clearly see that the non-efficient objects have a larger spread in their SFR^* than the efficient galaxies. The SFR^* of the latter sub-population are clustered at moderate values.

The star formation efficiency, ϵ, of a given galaxy is expected to be closely related to its color. Indeed, the instantaneous SFR is dominated by the youngest stellar populations and thus is a measure of the luminosity in the optical/UV bands. The galaxy mass is on the other hand a better measure of the luminosity in the infrared band, assuming some mass-to-light ratio, since the mass is the integration of all stellar populations produced over the lifetime of the galaxy. Low-mass galaxies of the simulated catalogs have the highest specific SFR^* and are thus expected to be bluer than massive galaxies; observations of compact galaxies show bluer colors and lower mass than high-mass disk-like starburst galaxies (Guzman et al. 1997).

The first observational results on GRB host galaxies provide important clues to their nature. Le Floc'h et al. (2003) showed that the hosts are faint in the K band, typical luminosities being about $0.1L_*$. Berger et al. (2003) have shown that the hosts are bluer than other sub-mm galaxies. Chary et al. (2002) considered 11 GRB host galaxies and derived extinction corrected SFR for seven of these hosts as well as mass, starburst age and internal extinction. Six of them have redshifts between 0.7 and 1.6, one is at a high redshift of $z = 3.4$. They derive UV and β-slope $SFRs$ in the range 0.2-70 $M_\odot$/yr for the hosts with redshifts around unity and more than 300 $M_\odot$/yr for the host with highest redshift. Using population synthesis spectral energy distributions they computed the mass of host galaxies and found them to be of rather low-mass, between 10^8 and $4 \cdot 10^9 M_\odot$ for the hosts with redshifts around unity. The host galaxy at $z = 3.4$ is a higher mass object, $3 \cdot 10^{10} M_\odot$. These mass values are also consistent with other estimates (Sokolov et al. 2001). As a result, Chary et al. (2002) estimate the specific star formation rate of these hosts, approximately in the range $\epsilon = 2.5 - 3.9$ in our units (see their fig. 2). Even with some uncertainties, these values are consistent with values inferred for star-bursting galaxies (see upper panel of fig. 16 in Pérez-González et al. (2003) based on observations by Calzetti (1997)). Future observations will reveal more details of the host galaxies and especially the connection these have with the observed population of blue galaxies, which could be irregulars, star-bursting, compact or HII.

Based on these host galaxy observations and on the fact that we can identify galaxy sub-populations in the simulations, we define our simulated candidate GRB host galaxies as efficiently star-forming objects, with high specific star formation rate (filled squares in fig. 8) A galaxy is considered a host if its efficiency is higher than $\bar{\epsilon}$, taken as the peak value of a given catalog. This value is rather arbitrary and is likely to be a lower limit, according to the observational estimate of the specific star formation rate in Christensen et al. (2004). The majority of these efficient galaxies in the simulations are low-mass objects, but a modest peak in the mass distribution around a few times $10^{10} M_\odot$ is also seen in the lower panel of fig. 9. Such galaxies are expected to be around 10 times less luminous than L_* galaxies, consistent with Le Floc'h et al. (2003). Moreover, the simulated host galaxy candidates are moderately active, with SFR^* spanning two orders of magnitude around unity. Their specific star formation rates spans about one order of magnitude (fig. 8). Most of these galaxies are also low-mass objects, clustering around the line representing $10^9 M_\odot$. This picture seems consistent with observations: Although the host galaxies in Chary et al. (2002) show much higher specific star formation rates than our candidates, it varies by a factor of 20 and the host masses are generally around 10^9 $M_\odot$. It is also interesting to note that one of their hosts with $z = 3.4$, has a similar ϵ as the hosts around $z = 1$, but with a much higher star formation rate and a galaxy mass that is two orders of magnitude higher. The simulations show a similar result, a 10^9 $M_\odot$ galaxy has a specific star formation rate in the range $\epsilon \approx 1.3 - 2.6$ at $z = 1$ (see fig. 8), which brackets the values obtained for a 10^{10} $M_\odot$ galaxy at $z = 3$ (fig. 6). Recall also, that the SFR^* increases at higher redshift for a given mass.

The location of the candidate host galaxies in the $\epsilon - SFR^*$ parameter space, appears to indicate that most of them would have high ϵ and modest to high SFR^*. This is also what the observations of Chary et al. (2002) show. Moreover, a number of hosts are classified as compact galaxies, and such galaxies appear to have SFR between 0.1 and 14 $M_\odot$/yr as in the sample of Guzman et al. (1997). Putting this together suggests that identifying host galaxies of GRBs as efficient galaxies provides us with first interpretations of the observations. Our results also point to a verifiable prediction regarding the observationally determined distribution of the specific star formation rates of GRB hosts. Observations of host galaxies could, however, be biased towards the most luminous objects and therefore the intermediate to high-mass range, with the more numerous and efficient, but much less massive, objects underrepresented. The solid histograms in fig. 10 show the efficiency distribution of the candidate host galaxies (i.e. objects with $\epsilon > \bar{\epsilon}$) at high and low redshifts. Considering all efficient objects results in broad distributions (solid histograms). If we now restrict the hosts to be the most massive of the efficient objects ($M > 10^{10} M_\odot$), we obtain strikingly different distributions. They are much narrower (dotted histograms) at both redshifts with the tail towards higher efficiency missing. First versions of observationally determined distributions similar to the dotted ones in fig. 10 already exist (Christensen 2002). The difference between the histograms, illustrate how our perception of the hosts will change if we are able to detect these low-mass galaxies.

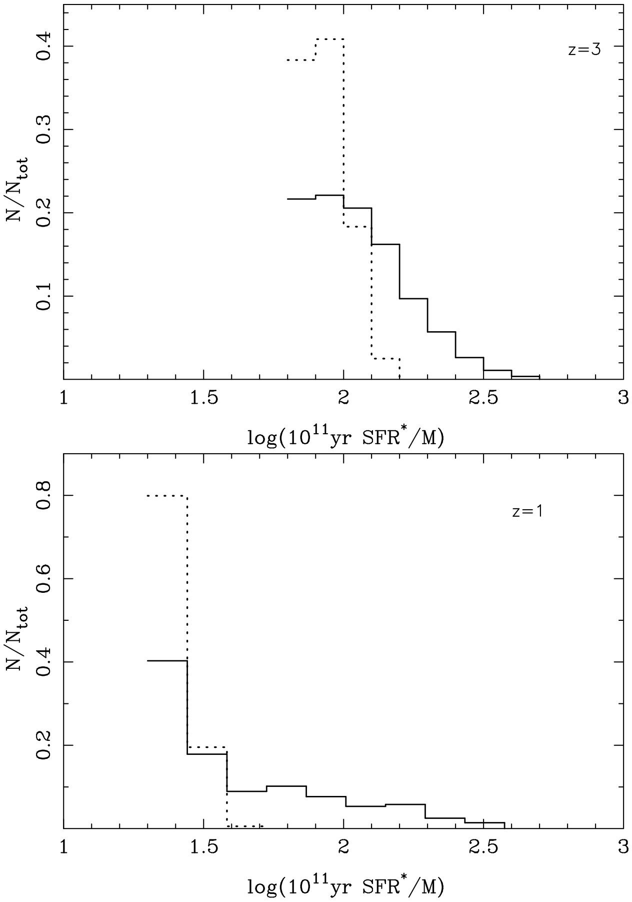

Figure 10. Upper panel: Number of host galaxies ($\epsilon > \bar{\epsilon} = 1.8$) per bin of specific star formation rate (solid histogram) compared to the distribution of host galaxies with $M > 10^{10} M_\odot$ (dotted histogram) at $z = 3$. Lower panel: same but at $z = 1$ with $\epsilon > \bar{\epsilon} = 1.3$. Histograms are normalized to the number of objects in each distribution.

The conclusion that host galaxies are, in majority, low-mass, late-formed galaxies with moderate star formation rates, derives from our hypothesis that candidate host galaxies are the most efficient ones. We adopted this hypothesis as observations indicate that the hosts have high specific star formation rates and moderate SFR (Christensen et al. 2004). Our conclusions would be different if the hypothesis is that candidate hosts are galaxies with the highest star formation rates, as may be expected if the GRB formation rate follows the global SFR. In that case, the majority of the host galaxies would be high-mass, inefficient, early-formed galaxies (see Fig. 8). It may be argued that for our adopted hypothesis to hold, and if GRBs trace the global SFR, low-mass galaxies should contribute significantly to the global star formation rate. However, inspection of Fig. 8, immediately shows that the matter is more complicated. If we select a sample of objects according to a particular criteria, we find that at $z = 1$, 50% of the total star formation rate is in galaxies with a $SFR^* < 9$ $M_\odot$/yr; or in galaxies with $\epsilon > 1.3$; or in galaxies with a mass less than $5 \cdot 10^{10} M_\odot$. Similarly at $z = 3$, these thresholds become $SFR^* = 17$

$M_\odot$/yr; or $\epsilon = 1.9$; or $M = 2 \cdot 10^{10} M_\odot$. Of course we have to keep in mind that these numerical values depend on the physics included in our simulations.

It is clear from Fig. 8 that if a higher specific star formation threshold is used to select candidate host galaxies, fewer hosts will have high SFR^*s. This would suggest that the GRB formation rate is not a tracer of the total star formation rate. The two rates follow each other (i) if the stellar mass function is independent of time and thus of the galaxy properties (such as mass, age, metal content, etc), and (ii) if the probability that a high-mass star gives birth to a GRB event is independent of time. Although a number of observational studies show that the stellar mass function depends on the galaxy type (Contini et al. 1995; Kroupa 2001; Larson 2003), most workers assume a universal initial mass function independent of time. Moreover, the underlying physics involved in the gamma-ray burst phenomena implies, among other things, that low-metalicity stars are favored. Such low-metalicity environments should mainly exist in young or starbursting or interacting galaxies rather than in evolved systems even if these may be forming high-mass stars. Similar caveats have been discussed in other contexts by Ramirez-Ruiz et al. (2002) and Choudhury & Srianand (2002). Observing host galaxies with properties such as a high specific star formation rate, could reinforce the fact that the probability of forming a GRB event from a high-mass star does depend on time and thus on the galaxy.

6 CONCLUSIONS

We have used numerical simulations of large scale structure formation to identify galaxy like objects and to follow their evolution. We concentrated on the mass, the epoch of formation and the instantaneous and specific star formation rates of the objects. Our most important results are as follows:

The whole galaxy population includes a significant number of low-mass objects with $M < 10^{10} M_\odot$. There is a strong cosmological evolution of the properties of the galaxy population between $z = 3$ and $z = 0$. We emphasize that the star formation rate of a galaxy should be considered a measure of its star formation *activity*, while the specific star formation rate is a measure of its star formation *efficiency*. These properties are nicely illustrated in a diagram of ϵ vs. SFR^* (fig. 8), where we find a number of clearly distinct sub-populations of galaxies.

The low-mass population is further divided into sub-populations, some of which have a high specific star formation rate. Based on these findings and on the first observational results of GRB hosts, we identify candidate hosts in the simulations as galaxies with high specific SFR^*, rather than objects with high star formation rate. The majority of these candidate host galaxies appear to be of low mass, with recent formation epochs and a moderate SFR^* of a few $M_\odot$/year or lower. The properties of the candidate hosts so identified, are consistent with the trends observed in the GRB host galaxies. An implication of our conclusions, given the applicability of the physical input in the simulations used here, is that GRBs may not trace the cosmic star formation rate.

Most of the observed GRB hosts to date have a redshift around unity. We show that the efficiency of the low-mass galaxies does not vary much with redshift. For high redshift, more and more galaxies are found to be efficient independent of mass, while the efficiency of intermediate to high-mass galaxies decreases strongly with decreasing redshift.

As the low-mass objects are very faint, the observations of GRB host galaxies will initially be observationally biased towards the intermediate and high-mass objects. These will be easier to detect due to their higher luminosity. They will typically have an SFR in the range $1 - 40 M_\odot$/year at a redshift of unity. It may take the next generation space telescopes to reveal the properties of the low-mass sub-population of host galaxies. These are expected to outnumber the currently observable hosts by a considerable factor.

Furthermore, the low-mass galaxy population is known to be important for the understanding of galaxy formation. GRB host galaxies may thus become useful tracers of this population or in fact the faint end of the galaxy luminosity function that may be difficult to detect otherwise. Thus GRB selected host galaxies may become an important link in the study of structure formation and evolution. Although GRB selected galaxies introduce its own 'selection effect', they are free from others affecting surveys of various kinds, such as the magnitude limited observations of optical surveys and the sensitivity limitation of the sub-mm observations.

ACKNOWLEDGMENTS

We thank the anonymous referee for constructive comments that helped improve the paper. This work was supported by a Special Grant from the Icelandic Research Council. The numerical simulations used in this paper were performed on NEC-SX5 at the Institut du Développement et des Ressources en Informatique Scientifique (France).

REFERENCES

Alimi J.-M., Courty S., 2004, A&A submitted

Bardeen J., Bond J., Kaiser N., Szalay A. S., 1986, ApJ, 304, 15

Berger E., Cowie L. L., Kulkarni S. R., Frail D. A., Aussel H., Barger A. J., 2003, ApJ, 588, 99

Blain A. W., Natarajan P., 2000, MNRAS, 312, L35

Bloom J. S., Djorgovski S. G., Kulkarni S. R., Frail D. A., 1998, ApJ, 507, L25

Bloom J. S., Frail D. A., Kulkarni S. R., 2003, ApJ, 594, 674

Bloom J. S. et al., 1999, ApJ, 518, L1

Brinchmann J., Ellis R. S., 2000, ApJ, 536, L77

Bunn E. F., White M., 1997, ApJ, 480, 6

Calzetti D., 1997, AJ, 113, 162

Castro-Tirado A. J. et al., 2001, A&A, 370, 398

Chary R., Becklin E. E., Armus L., 2002, ApJ, 566, 229

Christensen L., 2002, MS Thesis, University of Copenhagen

Christensen L., Hjorth J., Gorosabel J., 2004, A&A, submitted

Choudhury T. R., Srianand R., 2002, MNRAS, 336, L27

Contini T., Davoust E., Considere S., 1995, A&A, 303, 440

Courty S., Alimi J.-M., 2004, A&A 416, 875

Djorgovski S. G. et al., 2003, in Discoveries and Research Prospects from 6- to 10-Meter-Class Telescopes II. Edited by Guhathakurta, Puragra. Proceedings of the SPIE, Volume 4834 The cosmic gamma-ray bursts and their host galaxies in a cosmological context. pp 238–247

Fynbo J. U. et al., 2001, A&A, 373, 796

Giavalisco M., 2002, ARA&A, 40, 579

Guzman R., Gallego J., Koo D. C., Phillips A. C., Lowenthal J. D., Faber S. M., Illingworth G. D., Vogt N. P., 1997, ApJ, 489, 559

Hjorth J. et al., 2003, Nature, 423, 847

Hopkins A. M., Connolly A. J., Haarsma D. B., Cram L. E., 2001, AJ, 122, 288

Jaunsen A. O., Andersen M. I., Hjorth J., Fynbo J. P. U., Holland S. T., Thomsen B., Gorosabel J., Schaefer B. E., Björnsson G., Natarajan P., Tanvir N. R., 2003, A&A, 402, 125

Kroupa P., 2001, MNRAS, 322, 231

Lamb D. Q., Reichart D. E., 2000, ApJ, 536, 1

Larson R. B., 2003, in ASP Conf. Ser. 287: Galactic Star Formation Across the Stellar Mass Spectrum The Stellar Initial Mass Function and Beyond (Invited Review). pp 65–80

Le Floc'h E., Duc P.-A., Mirabel I. F., Sanders D. B., Bosch G., Diaz R. J., Donzelli C. J., Rodrigues I., Courvoisier T. J.-L., Greiner J., Mereghetti S., Melnick J., Maza J., Minniti D., 2003, A&A, 400, 499

Le Floc'h E., Duc P.-A., Mirabel I. F., Sanders D. B., Bosch G., Rodrigues I., Courvoisier T. J.-L., Mereghetti S., Melnick J., 2002, ApJ, 581, L81

Mészáros P., 2002, ARA&A, 40, 137

MacFadyen A. I., Woosley S. E., 1999, ApJ, 524, 262

Pérez-González P. G., Gil de Paz A., Zamorano J., Gallego J., Alonso-Herrero A., Aragón-Salamanca A., 2003, MNRAS, 338, 525

Paczyński B., 1998, ApJ, 494, L45

Padmanabhan T., 1993, Structure formation in the Universe. Cambridge University Press

Price P. A. et al., 2002, ApJ, 573, 85

Ramirez-Ruiz E., Trentham N., Blain A. W., 2002, MNRAS, 329, 465

Rees M. J., Ostriker J. P., 1977, MNRAS, 179, 541

Sokolov V. V. et al., 2001, A&A, 372, 438

Stanek, K. Z. et al., 2003, ApJ, 591, L17

Sugiyama N., 1995, ApJS, 100, 281

van Paradijs J., Kouveliotou C., Wijers R. A. M. J., 2000, ARA&A, 38, 379

Von Neumann J., Richtmyer R., 1950, J. Appl. Phys., 21, 232

Weinberg D. H., Hernquist L., Katz N., 2002, ApJ, 571, 15

Woosley S. E., 1993, ApJ, 405, 273